ACS APPLIED MATERIALS & INTERFACES

Research Article

www.acsami.org

Valence Band-Edge Engineering of Nickel Oxide Nanoparticles via Cobalt Doping for Application in p-Type Dye-Sensitized Solar Cells

Gayatri Natu, Panitat Hasin, Zhongjie Huang, Zhiqiang Ji, Mingfu He, and Yiying Wu*

Department of Chemistry & Biochemistry, The Ohio State University, 100 West 18th Avenue, Columbus, Ohio 43210, United States

Supporting Information

ABSTRACT: We have systematically studied the effects of substitutional doping of p-type nanoparticulate NiO with cobalt ions. Thin films of pure and Co-doped NiO nanoparticles with nominal compositions $Co_xNi_{1-x}O_y$ ($0 \leq x \leq 0.1$) were fabricated using sol–gel method. X-ray photoelectron spectroscopy revealed a surface enrichment of divalent cobalt ions in the $Co_xNi_{1-x}O_y$ nanoparticles. Mott–Schottky analysis in aqueous solutions was used to determine the space charge capacitance values of the films against aqueous electrolytes, which yielded acceptor state densities (N_A) and apparent flat-band potentials (E_{fb}). Both N_A and E_{fb} values of the doped NiO were found to gradually increase with increasing amount of doping; thus the Fermi energy level of the charge carriers decreased with Co-doping. The photovoltage of p-DSCs constructed using the $Co_xNi_{1-x}O_y$ films increased with increasing amount of cobalt, as expected from the trend in the E_{fb}. Co-doping increased both carrier lifetimes within the p-DSCs and the carrier transport times within the nanoparticulate semiconductor network. The nominal composition of $Co_{0.06}Ni_{0.94}O_y$ was found to be optimal for use in p-DSCs.

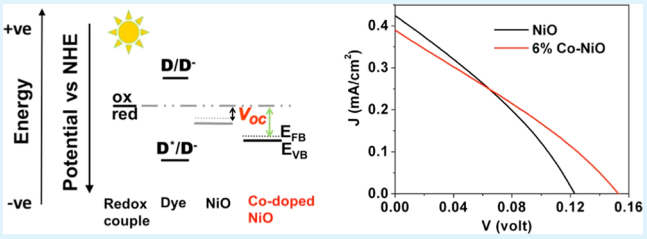

KEYWORDS: *nickel oxide, doping, dye-sensitized solar cells, Mott–Schottky, band tuning*

1. INTRODUCTION

Divalent nickel oxide (NiO) is one of the very few wide band gap p-type oxide semiconductors. The scarcity of p-type semiconducting nature in metal oxides has been explained on the basis of their electronic band structure.[1] Since the upper edge of the valence band in metal oxides is strongly localized on the oxide ions, the holes created in the valence band cannot be easily transported through the material. This is reflected in the typical values of Hall mobilities for NiO films (0.3 to 3.5 $cm^2 V^{-1} s^{-1}$)[2] versus those for n-type anatase TiO_2 films (20 $cm^2 V^{-1} s^{-1}$).[3] Thin films of NiO have been applied as hole-transport layers for many opto-electronic devices,[4−6] and NiO nanostructures have been extensively used to fabricate electrochemical supercapacitors[7,8] and p-type dye-sensitized solar cells (p-DSCs).[9] However, the poorer transport properties of NiO can limit the photocurrents in p-DSCs and lead to higher recombination (dark currents). Moreover, the open circuit voltages of NiO-based p-DSCs are limited by its valence band edge. As such, the best photoconversion efficiency of NiO-based p-DSC(0.41%)[10] is thirty times lower than the best efficiency of TiO_2-based n-DSC (12.3%).[11] Therefore, tuning the valence-band edge and improving the transport properties of NiO are important for improving the efficiency of NiO-based p-DSCs. Here, we present the first trial in this aspect.

There has been a division of opinion among researchers about the nature of carrier transport mechanism in nanoscale NiO.[12,13] The transport could take place through hole trapping and detrapping between the narrow valence band and the surface states or through small polaron hopping mediated via the surface states, although a consensus seems to be gathering around the latter mechanism. Emin[14] describes a small polaron as 'an extra electron or hole severely localized within a potential well that it creates by displacing the atoms that surround it'. Zhu et al. have proposed that the holes are present as Ni(III) at the surface of NiO nanoparticles, and the charge transport involves hopping of charges at the NiO/electrolyte interface.[15] Recent spectroelectrochemical studies performed in our research group also support the hopping mechanism, as the transport resistance in NiO-based p-DSCs is seen to be invariant with the incident photon intensity (manuscript in preparation).

The nature of carrier transport in nanoparticulate NiO is closely related to its charge carrier density and the structure of its valence band. To overcome the inherent limitations of carrier transport in nickel oxide, it is important to understand the microscopic origins of its electronic properties. One way to study a specific property of a system is to introduce a small perturbation in the system and examine the change in the property due to the perturbation. Point defects, such as dopants (intentionally introduced atomic impurities) or vacancies are known to create such perturbations and strongly affect the electronic properties of the materials.[16] We surmised that a systematic introduction of cationic dopants in the NiO crystal structure would be a viable method for the study of its transport

Received: August 5, 2012
Accepted: October 10, 2012
Published: October 10, 2012

   dx.doi.org/10.1021/am301565j | ACS Appl. Mater. Interfaces 2012, 4, 5922–5929

properties. Previous research on cationic doping of NiO has mainly focused on the magnetic,[17] dielectric[18−20] or conductivity measurements on microstructured thin films on NiO. Monovalent dopants, especially Li^+ ions, were generally found to increase the conductivity of the NiO films.[21−23] Among 3d transition metal dopants, Kim and Park reported an enhanced electrocatalytic activity in cobalt doped electrodeposited NiO films.[24] They observed higher oxidation states of Ni^{3+} and Ni^{4+} in the doped films via in situ XANES studies, indicative of an increased carrier concentration. Probing the fundamental properties such as the carrier density, chemical capacitance and the position of the valence band edge of the doped NiO could provide a sound explanation for such enhancement of device performance, and this was one motivation behind our study.

Additionally, the open circuit voltage of a photoelectrochemical cell such as a p-DSC constructed from NiO depends upon the relative position of its flat band potential (E_{fb}) and valence band edge (E_{VB}) to the Nernst potential of the redox couple in the cell. It has been shown that cationic doping in n-type semiconductors can have significant influence on their E_{fb} and conduction band edge (E_{CB}). Specifically, dopant atoms like Zr, Nb, and Ta have been introduced in TiO_2 nanostructures for tuning the band structure and improving n-DSC performance.[25−27]

NiO and CoO both have rock-salt structure, with lattice parameters 4.195 and 4.261 Å, respectively. The lattice mismatch between them is thus 1.6%, which is conducive to substitutional doping. The crystal ionic radii of both divalent and trivalent Co and Ni closely match each other.[28] Thus, it is possible to dope NiO with relatively high amounts of Co without causing much lattice strain, and a systematic study can be carried out with widely varying concentrations of the dopant ions. On the basis of these considerations, divalent cobalt was chosen as the initial candidate for our study of cationic doping in nanostructured NiO. Dye-sensitized cells fabricated from pure and doped NiO films were effectively utilized as devices to measure various electronic properties of the semiconductors.

2. RESULTS AND DISCUSSION

2.1. Structural Characterization. A simple sol−gel method was employed to synthesize nanoparticulate films of pure and cobalt-doped NiO (Experimental Section 4.2.1). In the usual manner of electrode preparation for sol−gel NiO-based p-DSCs, thin films from metal-chloride-based slurries were doctor-bladed onto conductively coated glass pieces and annealed at 450 °C in air. A scanning electron micrograph of NiO film is given in Figure S1 in the Supporting Information. Films were prepared with Co:Ni ratios varying from 1% to 20% in the initial precursors. The maximum doping amount for which the DSC film electrodes could be fabricated without losing the structural integrity of the films was 10% Co. Three distinct concentrations with low, intermediate and high dopant levels (2, 6, and 10%) were then chosen for further studies. We refer to these compositions as 2% Co, 6% Co, and 10% Co throughout the manuscript. However, it should be noted that these are *nominal* compositions of cobalt, based on the atomic percentage of Co with respect to Ni in the initial reagents. Figure 1 shows representative X-ray powder diffraction patterns of films deposited directly onto a glass sample-holder. The patterns showed no detectable peak shifts in 0, 2, to 10% Co, which indicates a substitutional doping, as expected.

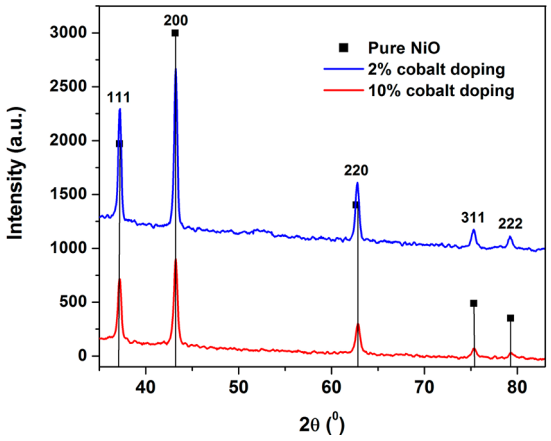

Figure 1. X -ray powder diffraction patterns for 2% and 10% cobalt-doped nickel oxide films used in this study, plotted against the peaks of the pure nickel oxide film. The intensity of the peaks of pure NiO is indicated by the heights of the lines corresponding to each peak. The peaks are indexed according to JCPDF file 65−2901.

2.2. X-ray Photoelectron Spectroscopy (XPS) Studies. XPS analysis was performed to study the surface compositions of the nanoparticulate films. The data for the 2% Co-doped film is not included in the analysis, as the cobalt signal was very weak for the films and the peaks could not be deconvoluted. Figure 2 shows the Ni 2p peaks for the pure and 6 and 10%

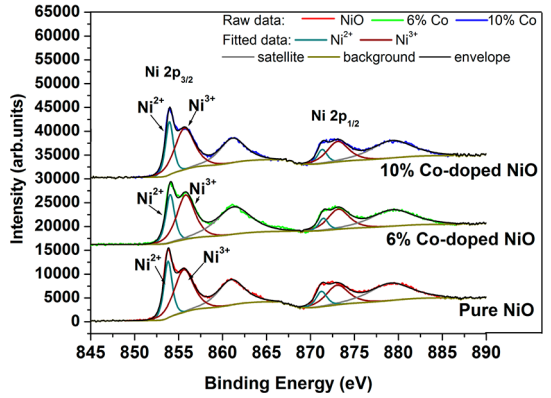

Figure 2. Ni 2p X-ray photoelectron spectra for pure and nominally 6% and 10% Co-doped nanoparticulate NiO.

nominally Co-doped samples. The peaks were fitted using a simple singlet envelope analysis, and the Ni^{2+}:Ni^{3+} ratios were found to be 0.531, 0.519, and 0.475 respectively. It should be noted that the Ni 2p photoelectron spectroscopy (PES) spectra is generally considered to require complex fitting methods, and the effect of nonlocal screening interactions might be considerable.[29] This has led some researchers to claim that the splitting of the Ni 2p peaks into divalent and trivalent nickel might be a phenomenon inherent to the PES analysis of divalent NiO, and does not necessarily imply that Ni^{3+} exists in such high amounts at the surface of NiO.[30] However, insertion of other divalent transition metal ions into rock-salt NiO lattice has been shown to decrease the nonlocal screening effects.[31]

A more discernible impact of the cobalt doping is seen through the Co 2p XPS plots for nominally 6% and 10% doped NiO (Figure 3). The overall amounts of cobalt ions at the surfaces of these compositions were 15.0% and 19.5% respectively. Such enrichment of cobalt at the surface of the

dx.doi.org/10.1021/am301565j | ACS Appl. Mater. Interfaces 2012, 4, 5922−5929

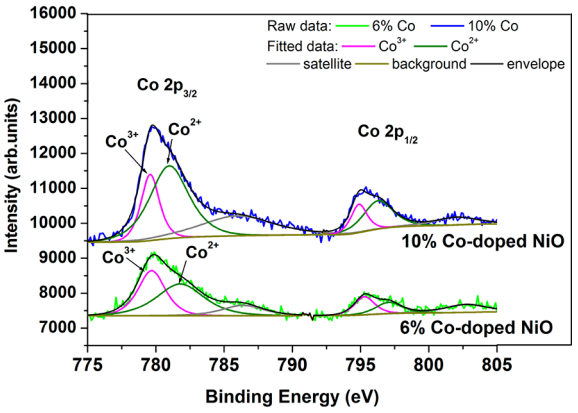

Figure 3. Co 2p X-ray photoelectron spectra for nominally 6% and 10% Co-doped nanoparticulate NiO.

nanoparticles is expected, as surface migration of dopant ions is frequently observed under annealing conditions.[32] The Co^{2+}:Co^{3+} ratios in these compositions were 1.12 and 1.35, respectively. These amounts translate to 7.92% and 11.2% of divalent cobalt atoms (as compared to all metal ions comprising the surface) of the nominally 6% and 10% doped NiO nanoparticles. The octahedrally coordinated Co^{2+} and Ni^{2+} ions are in high-spin configurations in their native oxides, and the Co^{2+} can accept one more electron in its t_{2g} levels than Ni^{2+}.[33] As such, the surface-enrichment of divalent cobalt would amount to extra density of acceptor levels in the NiO nanoparticles, as we have confirmed in section 2.2 through the Mott–Schottky measurements.

2.3. Mott–Schottky Measurements on the Nanoparticulate Films. "Mott–Schottky measurement" is a widely used technique for measuring the flat-band potentials (Fermi energy levels) and charge carrier densities of bulk semiconductors in contact with redox electrolytes. This technique involves the application of varying potential bias to the semiconductor–electrolyte interface and measurement of the space-charge capacitance within the semiconductor. For a p-type semiconductor, a plot of the inverse square of the capacitance (C_{sc}) versus the applied potential bias yields the flat-band potential E_{fb} according to the following equation:[34]

$$\frac{1}{C_{sc}^2} = \frac{-2}{e\varepsilon_0\kappa NA^2}\left(E - E_{fb} - \frac{k_B T}{e}\right) \quad (1)$$

where κ, N, and A are the dielectric constant, density of acceptors within the space charge region, and effective surface area of the semiconductor.

For a spherical nanoparticulate semiconductor of radius r in contact with an electrolyte, the maximum degree of band bending ($\Delta\phi_{sc}$) is given by[35]

$$\Delta\varphi_{sc} = \frac{eNr^2}{3\varepsilon_0\kappa} \quad (2)$$

In lightly doped semiconductors with a high dielectric constant, $\Delta\phi_{sc}$ can be negligibly small, so the Mott–Schottky analysis or the term E_{fb} does not yield meaningful results.[36] For example, the bands would bend only by 5 mV for a TiO_2 nanoparticle with a radius of 10 nm and a donor density of 1×10^{18} cm^{-3}, as the κ-value for titanium dioxide is 173. However, the dielectric constant of NiO is reported to be 11.9 at room temperature.[37] Chen et. al[38] have performed Hall measurements on sputter-deposited NiO nanoparticles with 15 nm radius, and obtained high carrier densities of 7.35×10^{18} cm^{-3}. The degree of band bending in such nanoparticles, according to eq 2, would be nearly 0.8 V. As the sol–gel synthesized nanoparticles in our report are in the same size regime, we expect a significant band bending within the materials.

We note that the Mott–Schottky analysis is valid only under the carrier depletion condition within the semiconductor.[39] In case of a p-type semiconductor like NiO, the depletion condition is achieved when holes from the semiconductor deplete into the electrolyte solution, bending the bands downward near the interface. Therefore, if a bias potential more negative than the fermi level of the p-type semiconductor is applied to the interface, the semiconductor would be in the depletion region. For each semiconductor film under study, we chose a wide range of applied bias (−0.3 to 0.6 V vs NHE) such that transition from the depletion to the flat band condition would be apparent in the Mott–Schottky plots. Sodium dihydrogen phosphate buffer was chosen as the electrolyte for maintaining a constant pH throughout the measurement. 1 M KCl was added as a supporting electrolyte to increase the conductivity of the solution and to ensure that the potential drop across the Gouy layer in the electrolyte can be

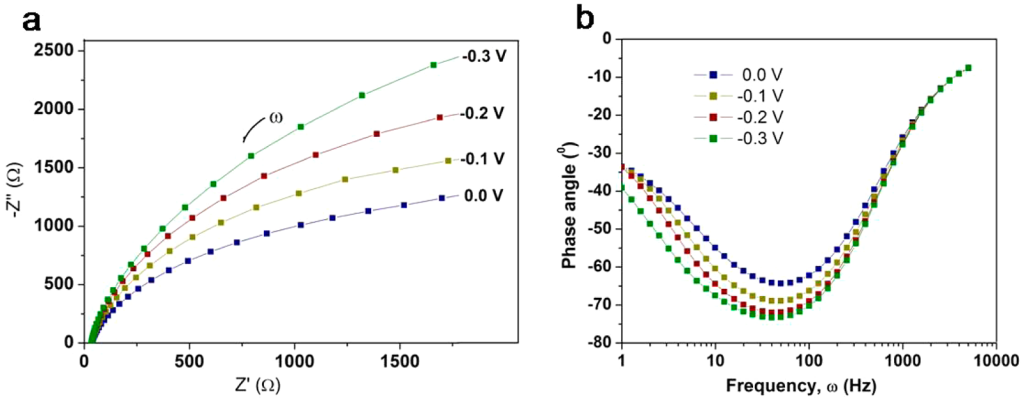

Figure 4. Representative (a) Nyquist plots and (b)Bode plots from the electrochemical impedance spectroscopy on doped NiO nanoparticulate film on FTO substrate in contact with an aqueous electrolyte of pH 7; The applied bias voltage (vs NHE) is noted against each plot. The frequency (ω) range for the measurements was 1 Hz to 10 kHz, and the arrow in a indicates the direction of increasing ω. The AC amplitude was 10 mV. Composition of the electrolyte: 0.1 M NaH_2PO_4 + 1 M KCl in deionized water.

neglected.[34] The differential capacitance measured across the semiconductor-electrolyte interface is thus a series combination of the Helmholtz capacitance (C_H) on the electrolyte side and the space charge capacitance (C_{SC}) on the semiconductor side. Typically for semiconductor-electrolyte interfaces, C_H is at least an order of magnitude larger than C_{SC}.[40] Therefore, the overall differential capacitance across the interface is dominated by the space-charge capacitance values within the semiconductor films. To measure this capacitance, we first plotted the electrochemical impedance spectra (EIS) for several values of applied bias potential within the frequency range of 1 Hz to 10 kHz. The representative EIS data for 2% Co-doped NiO are shown in Figure 4. The plot of frequency versus the phase angle of the circuit elements (Figure 4) indicates that the capacitive element in the circuit (phase angle near −90°) dominates at intermediate freqencies near 100 Hz. Therefore, capacitance values were obtained from a simple R−C circuit fitting to the impedance value obtained at 100 Hz for all electrode samples.

The differential capacitance thus obtained was approximated to C_{SC}. The surface roughness factor of the films was 33.9 as determined from the amount of adsorbed dye (SI-3). The inverse square values of area-normalized capacitance of the pure and Co-doped NiO films are plotted against applied bias potential in Figure 5 (Mott−Schottky plots), along with the

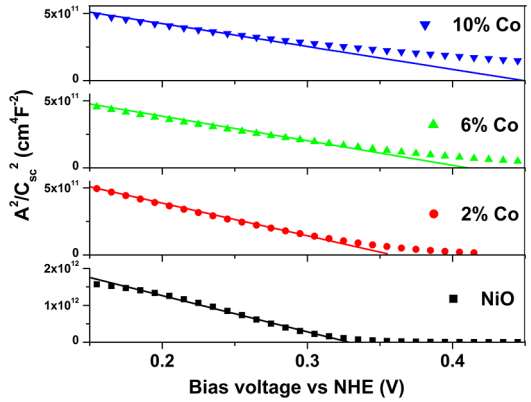

Figure 5. Mott−Schottky plots for pure and Co-doped nanoparticulate NiO films against an aqueous electrolyte containing 0.1 M NaH_2PO_4, 1 M KCl, and pH adjusted to 7.0.

linear fits in the depletion regions. The p-type semiconductor nature of the nanoparticulate films is confirmed by the negative slopes of the lines. The apparent flat-band potential corrected for the Boltzmann energy is calculated from the intercept on the abscissa, and the density of acceptor states from the slope of the fits. These values are tabulated in table 1.

We further tuned the pH of the phosphate-based aqueous electrolyte to two different values, one more acidic (4.2) and one more basic (9.0), and obtained Mott−Schottky plots of the semiconductors against these electrolytes. Figure 6 shows the pH dependence of flat band potentials. The E_{fb} values of pure and doped NiO decrease about 65 mV per unit of pH, which is close to the expected value of 59 mV per decade for an ideal semiconductor−aqueous electrolyte interface.[41]

The trend in the flat band potentials of the films at any given pH indicates that the Fermi energy of pure NiO is lowered by a few tens of millivolts upon cobalt doping. As shown below, the increase in the V_{oc} of the p-DSCs upon cobalt doping is consistent with this observtion. The acceptor density of NiO nanoparticles calculated in this report (1.2×10^{18} cm^{-3}) is of

Table 1. Values of Apparent Flat-Band Potentials at pH 7, Acceptor-State Densities, and Extrapolated Values for Valence Band Edge at pH 7 for Pure and Co-Doped Nanoparticulate NiO Films[a]

	E_{fb} (V vs NHE) measured at pH 7	N_A(× 10^{18}/ cm^3)	E_V (V vs NHE) extrapolated at pH 7
NiO	0.303 ± 0.013	1.21 ± 0.06	0.37
2% Co	0.333 ± 0.003	4.84 ± 0.1	0.38
6% Co	0.384 ± 0.005	6.46 ± 0.07	0.0.41
10% Co	0.423 ± 0.006	6.95 ± 0.12	0.45

[a]The E_{fb} values shift to more positive potentials with a higher level of cobalt doping.

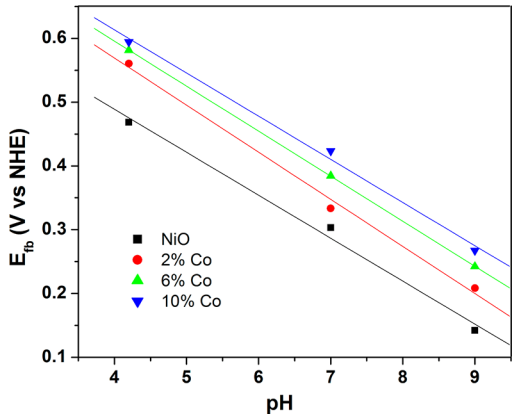

Figure 6. pH dependence of E_{FB} for pure and Co-doped nanoparticulate NiO films against an aqueous electrolyte containing 0.1 M NaH_2PO_4, 1 M KCl.

the same order of magnitude as the value previously reported for compact NiO films obtained via sputter deposition (7.35×10^{18} cm^{-3}) by Chen and coauthors.[38] Wilhelm and Hackerman measured the flat-band potential of NiO formed electrochemically on Ni surface,[42] using the photocurrent-onset method. Our value of E_{fb} of 0.303 V vs NHE at pH 7.0 for nanoparticulate NiO differs by 0.2 V from their measured value of 0.501 V vs NHE at pH 6.9.

The valence band edge of the nickel oxide nanoparticles can be determined from their flat band potentials, charge carrier density and effective hole mass from the following eqution[43]

$$p = 2\left(\frac{m_h^* k_B T}{2\pi\hbar^2}\right)^{3/2} \exp\left(-\frac{E_F - E_V}{k_B T}\right) \quad (3)$$

where p is the density of holes, m_h* is effective hole mass, E_v is valence band edge, and E_F is fermi energy of the semiconductor. If the acceptor density calculated from the Mott−Schottky plots is considered to be equal to the hole density, and the mass of the holes in pure and doped NiO is taken as 0.8 m_e,[5,44] the valence band edge for each composition can be calculated at pH 7. The values are reported in Table 1. The valence band edge potential for NiO (0.37 V vs NHE) is similar to the earlier values obtained via calculation[45] and experimentation.[46]

2.4. DSC Characterization. Dye-sensitized cells were fabricated from ∼600 nm thick, 0.5 × 0.5 cm^2 films of pure and Co-doped NiO on FTO-glass, sensitized with O2 dye,[47] as photocathodes (Experimental Section 4.2.3). The typical photoresponse of the cells under 1 sun AM1.5G illumination is shown in Figure 7 and quantified in Table S1 in the

dx.doi.org/10.1021/am301565j | ACS Appl. Mater. Interfaces 2012, 4, 5922−5929

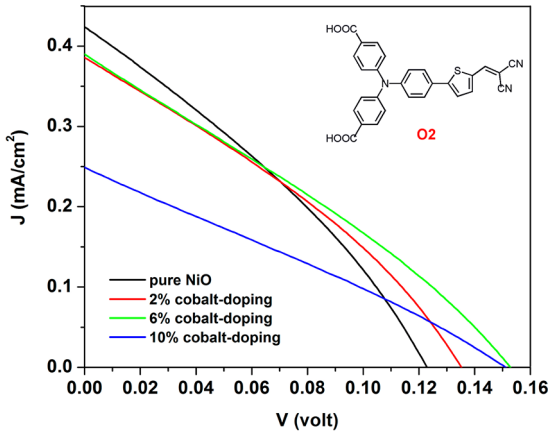

Figure 7. Typical photocurrent–voltage characteristics of p-DSCs constructed from the pure and cobalt-doped NiO films sensitized with O2 dye, under 1 sun intensity, with 0.1 M I_2 and 1 M LiI in 3-methoxypropionitrile as electrolyte. Film thickness: 0.6 μm.

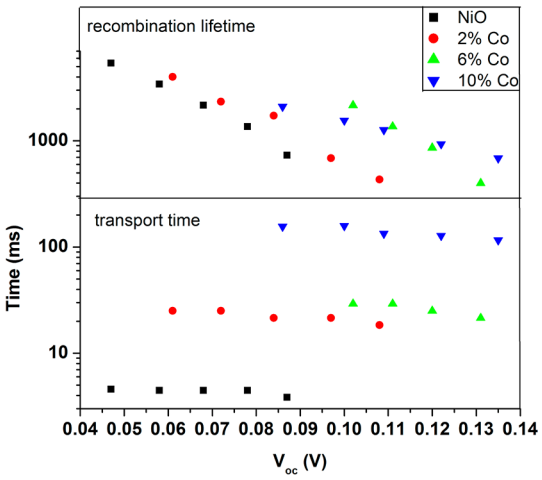

Figure 8. Hole transport times within the pure and Co-doped NiO-based p-DSCs plotted against short circuit photocurrents of the cells on a log–log scale. Carrier lifetimes (τ_{rec}) for the pure and Co-doped NiO-based p-DSCs plotted against open circuit photovoltages of the respectve cells on a semilog scale.

Supporting Information. Table S2 in the Supporting Information shows the average values of J_{sc} and V_{oc} values over three different batches of the cells.

The open circuit photovoltage V_{oc} of the DSCs is seen to increase from 122 mV in pure NiO to 138 mV in 2% Co-doped sample. A further increase to 158 mV is observed at 6% doping level, and then the V_{oc} remains at 157 mV for 10% Co- doped electrode. The gradual increase in V_{oc} values of the p-DSCs upon cobalt doping is directly in accordance with the trend in E_{fb} observed from our Mott–Schottky measurements in section 2.3.

The short circuit photocurrent density (J_{sc}) of the 2 and 6% Co-doped cells is slightly lower than that of the pure NiO cell; however, J_{sc} decreases drastically upon 10% doping of cobalt. We confirmed that this reduction of photocurrent did not result from a difference in the amount of adsorbed dye (the adsorption isotherm results are given in Figure S3 in the Supporting Information). The reduction of the photocurrent would result from excess scattering centers introduced into the lattice due to the high amount of dopant ions. This suggests that the carrier transport is much slower in NiO with high doping levels of cobalt.

The transport times (τ_{tr}) and the recombination lifetimes (τ_{rec}) of the charge carriers within the semiconductor network were obtained from intensity-modulated spectroscopies. A concise theoretical background on these techniques can be read from a review on electrons in nanostructured TiO_2 solar cells by Frank et. al.[48] Hole transport times in a p-DSC can be obtained from the intensity modulated photocurrent spectra (IMPS) while the hole lifetimes can be obtained from the intensity modulated photovoltage spectra (IMVS) of the p-DSCs, according to the relation $\tau = (1)/(2\pi\omega)$. We recorded IMPS and IMVS for p-DSCs based on pure and Co-doped NiO at varying incident intensity values. The peak frequency ω at each value of intensity was obtained from the highest magnitude of the transfer function in IMPS and IMVS. The logarithmic plots of transport times and lifetimes versus V_{oc} values for each cell are given in Figure 8. It should be noted that while the transport times are obtained under short circuit conditions, they are plotted against the open circuit voltage values from the corresponding I–V measurements for ease of comparison. The transport times are largely independent of the incident light intensity, except for the highest doped cell at high intensity values. The hole transport time in pure NiO cell is ~5 ms, which is in the range of carrier transport times observed for TiO_2-based n-DSCs,[49] despite the much thinner thickness of our NiO films. The transport times increase to more than 2-fold for 2% and 6% Co-doped NiO films. Such increase in the average transport time is expected for doped semiconductors, as the dopant ions act as scattering centers for the electrons or holes and reduce their mobility values. The transport times of the 10% Co-doped samples are increased by an order of magnitude, indicating a very large density of defects. The transport times for the cells are plotted on a log–log graph in Supporting Information, Figure S5. For the 10% Co-doped cell, an order of magnitude decrease in transport times (200 to 20 ms) is observed at the highest incident photon flux. This indicates that the carrier transport does not depend on the carrier concentration but rather on the mobility of the charge carriers.

The average lifetime of a charge carrier in the DSCs before it recombines is denoted as τ_{rec}, and is related to the resistance to recombination R_{rec} by the relation

$$\tau_{rec} = R_{rec} \cdot C_{\mu} \quad (4)$$

where C_{μ} is the chemical capacitance[50] of the photoelectrode. The exponential decrease in carrier lifetimes with increasing intensity of the incident light and the magnitudes of the lifetimes (a few hundred to a few thousand milliseconds) are in excellent agreement with previously reported results for NiO p-DSCs.[51] At identical values of the open circuit voltage, the hole lifetimes for 2% Co-doped cells are slightly higher than those for pure NiO cells. The τ_{rec} values increase even further for 6% doped cells, but decrease slightly at lower incident intensities upon 10% cobalt doping. The lifetimes of charge carriers in the 10% cobalt-doped samples are less dependent on the photon intensity than the lower doping levels, as seen from the relative slopes (Figure 8). However, the overall recombination lifetimes for the high cobalt-doped cells are still higher than the pure NiO based cells at a given photovoltage.

The relationship between the open circuit voltage V_{oc} of a solar cell is given by the diode equation[52]

dx.doi.org/10.1021/am301565j | ACS Appl. Mater. Interfaces 2012, 4, 5922–5929

$$V_{oc} = \frac{nkT}{e}\ln\left(\frac{J_{photo}}{J_0} + 1\right) \quad (5)$$

where n is the diode ideality factor, J_{photo} is the photocurrent density, and J_0 is the reverse saturation current density. As the photocurrent is proportional to the incident photon flux ϕ, at high ratios of J_{photo}/J_0, the V_{oc} is proportional to ϕ. The p-DSCs fabricated above were subjected to incremental changes in the incident intensity by using neutral density filters for the output of a 450 W Xe lamp, and the V_{oc} values were plotted against natural log of intensity (Figure 3). At each intensity, the trend of V_{oc} follows the pattern of $V_{oc\ (pure)} < V_{oc\ (2\%\ Co)} < V_{oc\ (6\%\ Co)} \sim V_{oc\ (10\%\ Co)}$. The ideality factors calculated from the slopes of these plots were 0.73, 0.75, 0.84, and 0.85, respectively, for the 0, 2, 6, and 10% cobalt-doped NiO electrodes, indicating an increase in the diode-like behavior with doping.

The dark current density of a DSC is a measure of J_0 or the "leakage current" of the cell. This current typically arises from dark recombination at the semiconductor-electrolyte junction. From eq 4, decreasing J_0 would increase the V_{oc}. The dark current in the p-DSCs at high potential bias indeed decreased with higher percent of cobalt doping (see Figure S2 in the Supporting Information). These observations point to an increased resistance to carrier recombination upon cobalt doping.

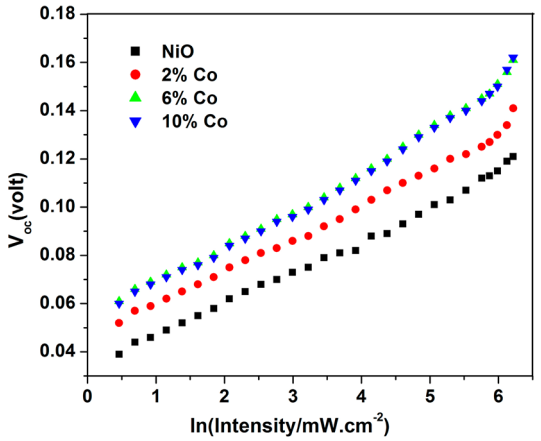

Figure 9. Intensity dependence of the photovoltage of the p-DSCs from Figure 1.

3. CONCLUSIONS

We have systematically doped nanoparticulate films of NiO with nominal doping compositions of 2, 6 and 10% cobalt. We found that the density of acceptor states around the valence band edge of NiO nanoparticles increases and the Fermi energy level is lowered gradually upon cobalt doping. The cobalt ions migrate to the surface of the nanoparticles and exist in both divalent and trivalent states. However, divalent cobalt predominates at higher nominal doping ratios, contributing to the acceptor states.

P-type dye sensitized solar cells were fabricated from the pure and Co-doped NiO films. The open-circuit voltage values increased with cobalt-doping, and the maximum increase was obtained for the nominally 6% doped films. The short-circuit photocurrent was reduced drastically for the 10% doped films despite the higher density of acceptor states (and consequently of holes). This phenomenon can be explained in terms of excess scattering centers introduced into the lattice and reducing the probability of polaron hopping. Higher incident photon flux might assist this type of carrier transport, resulting in lower transport times. This indicates that the carrier transport does not depend on the carrier concentration but rather on the mobility of the charge carriers. Therefore, bandlike carrier transport can be ruled out for NiO nanoparticles in favor of the small polaron hopping mechanism.

4. EXPERIMENTAL SECTION

4.1. Chemical Reagents. Following chemicals were used as received: Synperonic F-108, nickel chloride hexahydrate ($NiCl_2.6H_2O$), cobalt chloride hexahydrate ($CoCl_2.6H_2O$), sodium dihydrogen phosphate (NaH_2PO_4), sodium hydroxide (NaOH), potassium chloride (KCl), lithium iodide (LiI, 99.9%), iodine (I_2, 99.99%), 3-methoxypropionitrile(MPN), from Sigma-Aldrich; 200 proof ethyl alcohol and ACS grade isopropyl alcohol from Fisher Scientific. Aqueous solutions were prepared with deionized water (resistivity 18 MΩ.cm) from a Barnstead E-Pure system. Glass pieces ($2.5 \times 2.5 \times 0.3$ cm^3) coated with FTO (fluorine-doped tine oxide) from Hartford Glass Co. were used for the solar cell construction. The organic donor-π-acceptor type chromophore O2 was synthesized as described by Ji et. al.[47]

4.2. Procedural Details. *4.2.1. Materials Synthesis.* Pure and cobalt-doped NiO films were fabricated onto FTO-coated glass by modifying a method from Sumikura et. al.[53] For the precursor sol of pure NiO, 1.0 g of each of anhydrous $NiCl_2$ and F-108 were ground to a fine powder and dissolved in 3.0 g deionized water and 6.0 g ethanol. To obtain the precursors for the doped samples, stoichiometric amounts (2, 6, and 10 mol % Co:Ni ratio) of anhydrous $CoCl_2$ were added to the initial solutions. The solutions were kept undisturbed in a capped vial for three days at 30 °C. The resulting slurries were centrifuged to remove excess polymer. Films were fabricated in situ by coating the slurry onto FTO glass and annealing at 450 °C.

4.2.2. Electrochemical Measurements. A Reference 600 (Gamry Instruments) potentiostat was used to measure the potentiodynamic electrochemical impedance spectra of the pure and doped NiO films in aqueous electrolyte. The measurements were carried out in a custom-made Teflon cell, in a three-electrode configuration. The electrolyte used was a 0.1 M aqueous solution of sodium dihydrogen phosphate with 1 M potassium chloride as supporting electrolyte. The pH of the electrolyte was adjusted to 7.0 with sodium hydroxide. The reference electrode was Ag/AgCl in saturated KCl, and a porous graphite stick was used as the counter electrode. The reference and the counter electrodes were placed inside glass bridges fixed with fritted glass. After the assembly of the cell, Argon was passed for 20 min through the electrolyte to remove any dissolved oxygen. During measurements, a cover of argon was maintained above the surface of the electrolyte.

4.2.3. DSC Construction. Films were fabricated from the precursor slurry with the doctor blade technique: A "square well" of 0.5 cm edge length was constructed onto an FTO substrate using scotch tape. Ten μL of the slurry was placed on the scotch tape near the top of the defined area using a micropipet and was quickly spread onto the FTO using the sharp edge of a glass slide placed at an acute angle to the substrate. Care was taken not to allow a back-flow of the slurry onto the film. The scotch tape was removed and the films were kept in air for 30 min for drying. All films were then sintered at 450 °C for 90 min. A second layer of NiO was deposited by repeating the procedure. The films were then cooled to 120 °C and held at that temperature until their immersion in the dye solution. Dye sensitization was accomplished by immersing a film in a 0.3 mM solution of O2 dye in dry acetonitrile, kept inside a screw-capped vial away from ambient light for 24 h. Since the film thickness is subject to the exact concentration of the slurry and the heat treatment conditions, care was taken to use the pure and doped NiO films from the same batch for a given set of comparative experiments. Each experiment was performed

dx.doi.org/10.1021/am301565j | ACS Appl. Mater. Interfaces 2012, 4, 5922−5929

at least three times in order to account for the unavoidable variations in the films.

A typical solar cell was assembled by placing a platinum-coated conducting glass with a hole drilled into it on the dye-sensitized electrode separated by a 60 μm meltonix polymer spacer (Solaronix SA, Switzerland). The cell was sealed first by heating at 120 °C for 5 min and then applying an epoxy−resin sealant along its edges. An electrolyte was made with 1.0 M LiI and 0.1 M I_2 in dry methoxypropionitrile. The electrolyte was injected into the cell via vacuum backfilling through the drilled hole and the hole was again sealed using meltonix film, a thin glass cover slide and a quick-dry sealant.

4.2.4. DSC Characterization. Photovoltaic characterization was performed under 1 sun AM 1.5G simulated sunlight (Small-Area Class-B Solar Simulator, PV Measurements). $J-V$ curves were recorded with a CV-50W voltammetric analyzer. For measuring the intensity dependence of V_{oc}, the output intensity of a 450 W Xe lamp was modulated by using neutral density filters. A cooling fan was placed behind the test devices during these measurements to avoid heating of the cells. The Electrochemical Impedance Spectroscopy (EIS) data was obtained with a Gamry 600 reference potentiostat. The frequency range used for the scans was 30 kHz to 1 Hz, and the voltage perturbation amplitude was 10 mV. A Compactstat instrument (Ivium Technologies) was used for intensity-modulated photocurrent and photovoltage spectroscopy (IMPS and IMVS) measurements.

4.2.5. XPS Analysis. X-ray photoelectron spectroscopy measurements were performed on thin films of pure and Co-doped NiO deposited onto silicon substrates using a Kratos Axis Ultra XPS instrument. The Photoelectron excitation processes were initiated using an Al Kα source (energy 1486.6 eV). The vacuum in the analysis chamber was maintained at 1×10^{-9} Torr. Kratos Vision 2 software was used to perform curve fitting using a Gaussian−Lorentzian model. The C 1s peak (285 eV) was taken as the reference for the binding energy.

■ ASSOCIATED CONTENT

Supporting Information

SEM image of a NiO film; table of V_{oc}, J_{sc}, FF, and efficiencies of our p-DSCs; The dark $J-V$ curves of the cells; dye-adsorption isotherm measurements; recombination lifetime measurements from electrochemical impedance spectroscopy; carrier transport times plotted against short circuit photocurrent density. This material is available free of charge via the Internet at http://pubs.acs.org.

■ AUTHOR INFORMATION

Corresponding Author

*Phone: (+1) 614-247-7810. Fax: (+1) 614-292-1685. E-mail: wu@chemistry.ohio-state.edu.

Notes

The authors declare no competing financial interest.

■ ACKNOWLEDGMENTS

The authors acknowledge the funding support from the U.S. Department of Energy (Award DE-FG02-07ER46427).

■ REFERENCES

(1) Kawazoe, H.; Yasukawa, M.; Hyodo, H.; Kurita, M.; Yanagi, H.; Hosono, H. *Nature* **1997**, *389*, 939.
(2) Tyagi, M.; Tomar, M.; Gupta, V. *Anal. Chim. Acta* **2012**, *726*, 93.
(3) Ohno, K.; Tanaka, M.; Takeda, J. *Nano- and Micromaterials*; Springer, 2008; Vol. *9*.
(4) Caruge, J. M.; Halpert, J. E.; Bulovic, V.; Bawendi, M. G. *Nano Lett.* **2006**, *6*, 2991.
(5) Irwin, M. D.; Servaites, J. D.; Buchholz, D. B.; Leever, B. J.; Liu, J.; Emery, J. D.; Zhang, M.; Song, J. H.; Durstock, M. F.; Freeman, A. J.; Bedzyk, M. J.; Hersam, M. C.; Chang, R. P. H.; Ratner, M. A.; Marks, T. J. *Chem. Mater.* **2011**, *23*, 2218.
(6) Bandara, J.; Weerasinghe, H. *Sol. Energy Mater. Sol. Cells* **2005**, *85*, 385.
(7) Lu, Q.; Lattanzi, M. W.; Chen, Y. P.; Kou, X. M.; Li, W. F.; Fan, X.; Unruh, K. M.; Chen, J. G. G.; Xiao, J. Q. *Angew. Chem., Int. Ed.* **2011**, *50*, 6847.
(8) Liang, K.; Tang, X. Z.; Hu, W. C. *J. Mater. Chem.* **2012**, *22*, 11062.
(9) Odobel, F.; Le Pleux, L. c.; Pellegrin, Y.; Blart, E. *Acc. Chem. Res.* **2010**, *43*, 1063.
(10) Nattestad, A.; Mozer, A. J.; Fischer, M. K. R.; Cheng, Y. B.; Mishra, A.; Bauerle, P.; Bach, U. *Nat. Mater.* **2010**, *9*, 31.
(11) Yella, A.; Lee, H. W.; Tsao, H. N.; Yi, C. Y.; Chandiran, A. K. *Science* **2011**, *334*, 1203.
(12) Lunkenheimer, P.; Loidl, A.; Ottermann, C. R.; Bange, K. *Phys. Rev. B* **1991**, *44*, 5927.
(13) Wakefield, G.; Dobson, P. J.; Foo, Y. Y.; Loni, A.; Simons, A.; Hutchison, J. L. *Semicond. Sci. Technol.* **1997**, *12*, 1304.
(14) Emin, D. *Phys. Today* **1982**, *35*, 34.
(15) Zhu, H.; Hagfeldt, A.; Boschloo, G. *J. Phys. Chem. C* **2007**, *111*, 17455.
(16) Tuller, H. L.; Bishop, S. R. *Ann. Rev. Mater. Res., Vol 41* **2011**, *41*, 369.
(17) Yan, W. S.; Weng, W. X.; Zhang, G. B.; Sun, Z. H.; Liu, Q. H.; Pan, Z. Y.; Guo, Y. X.; Xu, P. S.; Wei, S. Q.; Zhang, Y. P.; Yan, S. S. *Appl. Phys. Lett.* **2008**, 92.
(18) Lin, Y. H.; Wang, J. F.; Jiang, L.; Chen, Y.; Nan, C. W. *Appl. Phys. Lett.* **2004**, *85*, 5664.
(19) Thongbai, P.; Pongha, S.; Yamwong, T.; Maensiri, S. *Appl. Phys. Lett.* **2009**, *94*.
(20) Wu, P.; Ligatchev, V.; Yu, Z. G.; Zheng, J. W.; Sullivan, M. B.; Zeng, Y. Z. *Phys. Rev. B* **2009**, *79*.
(21) Huang, Y. W.; Zhang, Q.; Xi, J. H.; Ji, Z. G. *Appl. Surf. Sci.* **2012**, *258*, 7435.
(22) Chen, S. C.; Kuo, T. Y.; Lin, Y. C.; Lin, H. C. *Thin Solid Films* **2011**, *519*, 4944.
(23) Turky, A. M. *Appl. Catal., A* **2003**, *247*, 83.
(24) Kim, J. W.; Park, S. M. *J. Electrochem. Soc.* **2003**, *150*, E560.
(25) Durr, M.; Rosselli, S.; Yasuda, A.; Nelles, G. *J. Phys. Chem. B* **2006**, *110*, 21899.
(26) Nikolay, T.; Larina, L.; Shevaleevskiy, O.; Ahn, B. T. *Energy Environ. Sci.* **2011**, *4*, 1480.
(27) Feng, X. J.; Shankar, K.; Paulose, M.; Grimes, C. A. *Angew. Chem., Int. Ed.* **2009**, *48*, 8095.
(28) Shannon, R. *Acta Cryst. A* **1976**, *32*, 751−767.
(29) Grosvenor, A. P.; Biesinger, M. C.; Smart, R. S.; McIntyre, N. S. *Surf. Sci.* **2006**, *600*, 1771.
(30) Gupta, P.; Dutta, T.; Mal, S.; Narayan, J. *J. Appl. Phys.* **2012**, 111.
(31) Gaskell, K. J.; Starace, A.; Langell, M. A. *J. Phys. Chem. C* **2007**, *111*, 13912.
(32) Soo, Y. L.; Wu, T. S.; Wang, C. S.; Chang, S. L.; Lee, H. Y.; Chu, P. P.; Chen, C. Y.; Chou, L. J.; Chan, T. S.; Hsieh, C. A.; Lee, J. F.; Kwo, J.; Hong, M. *Appl. Phys. Lett.* 2011, *98*.
(33) Radwanski, R. J.; Ropka, Z. *Phys. B: Condens. Matter* **2004**, *345*, 107.
(34) Rajeshwar, K. *Fundamentals of Semiconductor Electrochemistry and Photoelectrochemistry*; Wiley: New York, 2002; Vol. *6*.
(35) Watson, D. F.; Meyer, G. J. *Annu. Rev. Phys. Chem.* **2005**, *56*, 119.
(36) Quintana, M.; Edvinsson, T.; Hagfeldt, A.; Boschloo, G. *J. Phys. Chem. C* **2007**, *111*, 1035.
(37) Rao, K. V.; Smakula, A. *J. Appl. Phys.* **1965**, *36*, 2031.
(38) Chen, H. L.; Yang, Y. S. *Thin Solid Films* **2008**, *516*, 5590.
(39) Bott, A. *Curr. Separations* **1998**, *17*, 87.
(40) van de Krol, R.; Gratzel, M., Eds. *Photoelectrochemical Hydrogen Production*; Electronic Materials: Science & Technology; Springer: New York, 2012; Vol. *102*, p 41

(41) Gerischer, H. *Electrochim. Acta* **1989**, *34*, 1005.
(42) Wilhelm, S. M.; Hackerman, N. *J. Electrochem. Soc.* **1981**, *128*, 1668.
(43) Grundmann, M. *The Physics of Semiconductors*; Springer: New York, 2010.
(44) Choi, S. C.; Koumoto, K.; Yanagida, H. *J. Mater. Sci.* **1986**, *21*, 1947.
(45) Koffyberg, F.; Benko, F. *J. Electrochem. Soc.* **1981**, *128*, 2476.
(46) Nakaoka, K.; Ueyama, J.; Ogura, K. *J. Electroanal. Chem.* **2004**, *571*, 93.
(47) Ji, Z.; Natu, G.; Huang, Z.; Wu, Y. *Energy Environ. Sci.* **2011**, *4*, 2818.
(48) Frank, A. J.; Kopidakis, N.; van de Lagemaat, J. *Coord. Chem. Rev.* **2004**, *248*, 1165.
(49) Van der Zaden, B.; Goossens, A. *J. Phys. Chem. B* **2000**, *104*, 7171.
(50) Bisquert, J. *Phys. Chem. Chem. Phys.* **2003**, *5*, 5360.
(51) Huang, Z.; Natu, G.; Ji, Z.; Hasin, P.; Wu, Y. *J. Phys. Chem. C* **2011**, *115*, 25109.
(52) Natu, G.; Huang, Z.; Ji, Z.; Wu, Y. *Langmuir* **2011**, *28*, 950.
(53) Sumikura, S.; Mori, S.; Shimizu, S.; Usami, H.; Suzuki, E. *J. Photochem. Photobiol., A* **2008**, *199*, 1.